Accurate Quasi-TEM Spectral Domain Analysis of Single and Multiple Coupled Microstrip Lines of Arbitrary Metallization Thickness

Jen-Tsai Kuo, *Member, IEEE*

Abstract—**The quasi-TEM spectral domain approach (SDA) is extended to rigorously and efficiently analyze single and multiple coupled microstrip lines of arbitrary metallization thickness. The charge distributions on both the horizontal and vertical conductor surfaces are modeled by global basis functions. This results in a relatively small matrix for accurate determination of the line parameters of coupled thick microstrips. A convergence study is performed for the results of a pair of coupled lines with crucial structural parameters to explore the conditions for obtaining reliable solutions using the technique. Results for thick microstrips are validated through comparison with those from available measurements and another theoretical technique. The soundness of the technique is further demonstrated by looking into the trend of the results obtained by a simplified model in which the structural parameters are pushed, step by step, to the numerical extremities. Variations of circuit parameters of a four-line coupled microstrip structure due to the change of finite metallization thickness are presented and discussed.**

I. Introduction

THE MICROSTRIP line is widely recognized as the planar transmission line most extensively used and analyzed [1]. Many analyses of planar transmission lines are based on an assumption that the metallic strips are of zero thickness because this can simplify the electromagnetic formulation. Finite metallization thickness, however, is one of several important factors that affect the propagation properties of microstrip lines, since it must influence the field distribution around the strip. Typical examples are the microstrips designed to carry at least moderate power in microwave integrated circuits (MIC's) [2] and narrow but relatively thick conductors used as waveguiding media in high-density miniaturized monolithic microwave integrated circuits (MMIC's).

Some full-wave approaches [3]–[5] have been developed to analyze the finite thickness microstrip lines for applications at high frequencies. However, most of the analyses [6]–[13] are based on quasi-TEM formulations since the results are acceptably accurate at low frequencies and easy to obtain.

The conformal mapping method [6] has played a fundamental role in the development of microstrip line analysis. Later, the Green's function method [7] and the boundary element method [8] have also been formulated to tackle thick microstrips in a metallic enclosure.

The technique presented in [9] is the prelude to a widely adopted spectral domain approach (SDA) used in analyzing planar transmission lines. The SDA is superior to many numerical methods in the spatial domain [14] because of its ease of formulation, numerical efficiency, and good accuracy. The SDA formulation for rigorously analyzing planar waveguiding structures, however, has hitherto been restricted to infinitely thin strips.

Recently, the circuit parameters of stratified dielectric structures with rectangular and trapezoidal strip cross sections have been calculated based on a two-level model [10] and a multistrip model [11]. The accuracy of the two-level model has been validated against measured results for moderately thick coupled strips. It is obvious that the multistrip model is more suitable for strips with further thickness. However, in some special MIC and MMIC designs, e.g., directional couplers of high coupling parameters [2] or filters of wide bandwidth, the gap of the parallel coupled strips may become much narrower than the width. Under this circumstance, it becomes a challenge to obtain accurate results using these models. This is because the contributions from the charges on adjacent strip sidewalls to the propagation charactristics can become dominant, and the matching quality of the boundary condition over there is critical in determining the line parameters. We will address this issue in greater detail later.

Also of interest are the works presented in [12], [13]. Olyslager [12] tackles the general multiconductor transmission lines by a new and fast algorithm. Gentili [13] analyzes planar transmission lines with finite thickness based on a mixed spectral-space domain representation of the Green's function. It is worth mentioning that in works [11]–[13], with the aid of the Green's function in the spectral domain and the inverse Fourier transform, the spatial Green's function is invoked to set up an integral equation. Then discretized basis functions are adopted to model the unknown charge distributions and to reduce the integral equation to a matrix equation via the point-matching method [11], [12] or the Galerkin's technique [13]. Note that the order of the matrix in the final matrix equation, which is reduced from the integral equation, is proportional to the number of discretized bases used for each conductor.

This purpose of this paper is to extend the standard SDA formulation, incorporated with a set of global basis functions,

Manuscript received August 1, 1994; revised April 24, 1995. This work is supported in part by the National Science Council, Taiwan, R.O.C., Grant NSC 83-0404-E-009-124.

The author is with the Department of Communication Engineering, National Chiao Tung University, Hsinchu, Taiwan, R.O.C.

IEEE Log Number 9412667.

to analyze microstrip lines of rectangular cross sections. Analytical Fourier transform is invoked for each global basis function, whereas the process of the inverse Fourier transform is not necessary (as guaranteed by the Parseval's theorem via the application of Galerkin's procedure).

It is the use of global basis functions that results in a relatively small matrix in the final matrix equation. It will be shown later that the price paid for this is the involvement of certain single and double integrals. The evaluations of these integrals may be detrimental to efficiency, one of the key inherent advantages of the SDA technique. To maintain efficiency, an interpolation formula is used to evaluate the integrals based on a database in readiness. As a result, the efficiency of the method is greatly improved.

The presentation is organized as follows. Section II formulates the SDA for multiple coupled microstrip lines of arbitrary metallization thickness. Section III describes the global basis functions used in the analysis and the details for tackling the single and double integrals. In Section IV, a convergence study of the circuit parameters for a pair of coupled lines with crucial structural parameters is performed to explore the conditions for obtaining reliable field solutions. An extensive investigation into the multistrip modeling is done to demonstrate the soundness of the proposed technique in analyzing coupled microstrip lines with highly metallized thickness and close proximity. Calculated characteristic impedances for thick microstrips are compared with the available measured data and by another analysis technique. Finally, the circuit parameters of multiple coupled microstrip lines in response to the variation of metallization thickness are presented.

II. Formulation

In Fig. 1, the rectangular boxes sitting on the subtrate stand for the analyzed perfectly conducting multiple coupled microstrips of finite metallization thickness t. The cross sectional electrostatic field solution of the multiconductor transmission-line structure is governed by the Poisson's equation

$$(\partial^2/\partial x^2 + \partial^2/\partial y^2)\phi(x, y) = -\rho(x, y)/\epsilon(y) \qquad (1)$$

where $\phi(x, y)$ is the potential function and $\rho(x, y)$ the charge density distribution. The first step of the SDA is to apply the Fourier transform to the field quantities in (1). Consider the coupled microstrips in Fig. 1 as a multilayr multiconductor structure, in which the line sources are placed at $y = 0$, ξ, and t. The spectral Green's function at each interface with source can be written as [10]

$$G(\alpha_n, y; \xi) = A_n(\xi)\sinh(\alpha_n y) + B_n(\xi)\cosh(\alpha_n y), \quad 0 \le y \le t. \qquad (2)$$

Since all the mathematical manipulations in the spectral domain deal with the same spectral variable, α_n, it is suppressed in the field expressions herein. Note that the charge densities on each conducting surface are continuously distributed. Thus, to calculate the spectral potential functions for $0 \le y \le t$, the

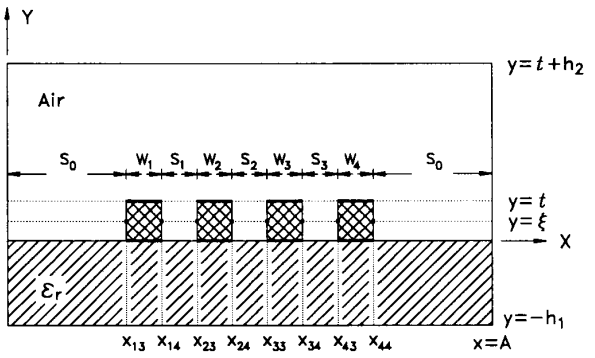

Fig. 1. Structure of the analyzed multiple coupled thick microstrip lines.

contributions from the charge densities on the vertical surfaces should be superimposed for all possible ξ, in addition to those on the horizontal ones. It leads to

$$\tilde{\phi}_{ij}(y) = \sum_{k=1}^{2} \tilde{G}_{jk}(y)\left(\sum_{l=1}^{N_c}\tilde{\rho}_{lk}\right) + \sum_{k=3}^{4}\int_0^t \tilde{G}_{jk}(y, \xi)\left(\sum_{l=1}^{N_c}\tilde{\rho}_{lk}(\xi)\right) d\xi, \qquad 1 \le j \le 4 \quad (3)$$

where the overhead tilt represents the transform of the corresponding field quantity, the subscripts i and l denote the orders of conductors, and j and k are used to identify the conductor surfaces. Surfaces 1 and 2 are those at $y = t$ and $y = 0$, respectively. $\tilde{\phi}_{i3}$ and $\tilde{\phi}_{i4}$ are the spectral potential functions on the surfaces at $x = x_{i3}$ and $x = x_{i4}$, respectively. $\tilde{\rho}_{lk}$'s are the transformed unknown charge distribution functions on conductor surfaces and N_c is the number of conductors in the structure. The Green's function $\tilde{G}_{jk}$ denotes the potential on the jth surface in response to the delta source on the kth one. For $j \ge 3$ and $k \ge 3$, the Green's functions have different expressions for $y > \xi$ and $y < \xi$ to account for the field point being above or below the source.

The Galerkin's technique is used to set up the final matrix equation. The unknown charge distributions are expanded in terms of known basis functions, namely

$$\rho_{ij}(\zeta) = \sum_{m=1}^{K_b} a_{ijm}\rho_{ijm}(\zeta) \qquad (4)$$

where a_{ijm}'s are the unknown constants to be solved, and K_b is the number of basis functions used to model the charge distribution on each surface. Substituting (4) into (3), multiplying both sides by $\tilde{\rho}^*_{ijm}$, and taking summations with respect to the discrete values of α_n for $n = -\infty$ to $+\infty$, one obtains

$$\frac{V_i}{A}Q_{ijm} = \sum_{n,p,l}\left\{\sum_{k=1}^{2} a_{lkp}\tilde{G}_{jk}\tilde{\rho}_{lkp} + \sum_{k=3}^{4} a_{lkp}\int_0^t \tilde{G}_{jk}(\xi)\tilde{\rho}_{lkp}(\xi)\, d\xi\right\}\tilde{\rho}^*_{ijm} \qquad (5a)$$

for $j = 1$ and 2, and

$$\frac{V_i}{A}Q_{ijm} = \sum_{n,p,l}\left\{\sum_{k=1}^{2} a_{lkp}\tilde{\rho}_{lkp}\int_0^t \tilde{G}_{jk}(y)\tilde{\rho}^*_{ijm}(y)\,dy + \sum_{k=3}^{4} a_{lkp}\int_0^t\int_0^t \tilde{G}_{jk}(y,\xi)\tilde{\rho}_{lkp}(\xi)\tilde{\rho}^*_{ijm}(y)\,d\xi\,dy\right\} \quad (5b)$$

for $j = 3$ and 4, after both sides are further integrated from $y = 0$ to $y = t$. Here, V_i is the potential of the ith conductor, Q_{ijm} is the area covered by the basis function ρ_{ijm}, and the superscript asterisk denotes the complex conjugate. The left-hand side of (5) is obtained via the Parseval's theorem [7].

The simultaneous equations in (5) for all different values of i, j and m give the final matrix equation

$$\underline{M}\,\underline{a} = \underline{d} \quad (6)$$

where $\underline{d}$ is a column vector of size $4N_cK_b$, and the entries of the constant vector $\underline{a}$ are the expansion coefficients of the basis functions. Note that if the entries involving single and double integrals, which represent the contributions of the charge distributions on vertical surfaces, are removed from $\underline{M}$, the matrix equation is reduced to that obtained by the two-level model [10]. The numerical treatments of the involved integrals will be reported in the next section.

After the vector $\underline{a}$ is obtained from (6), the entries of distributed capacitance matrix $\underline{C}$ can be calculated via

$$C_{il} = \left.\frac{Q_i}{V_l}\right|_{V_k=0,k\neq l} \quad (7)$$

where Q_i is the total charge on the ith conductor due to the potential excitation V_l. The inductance matrix $\underline{L}$ is calculated as the inverse of $\underline{C}$ with the dielectric layer being replaced by air. It is known that there are N_c eigenmodes that propagate along the multiconductor transmission-line. The effective dielectric constant for each eigenmode and the associated eigenvoltage vector are respectively the eigenvalue and eigenvector of the matrix product $\underline{L}\,\underline{C}$. The eigencurrent vectors are the eigenvectors of the product $\underline{C}\,\underline{L}$. Let $\underline{M}_V$ ($\underline{M}_I$) be the eigenvoltage (eigencurrent) matrix of which each column is the eigenvoltage (eigencurrent) vector. Then the characteristic conductance matrix $\underline{G}$ is $\underline{M}_I$ postmultiplied by $\underline{M}_V^{-1}$. The characteristic impedance matrix is the inverse of $\underline{G}$. When $N_c = 1$, the effective dielectric constant and the characteristic impedance reduce to

$$\epsilon_{reff} = C/C_o, \qquad Z_o = [\nu_c(CC_o)^{1/2}]^{-1}(\Omega) \quad (8)$$

where C_o is the distributed capacitance for $\epsilon_r = 1$, and ν_c the velocity of light in free space.

III. The Global Basis Functions and Numerical Details

Since the SDA formulation for analyzing the coupled thick microstrips is analytical, the accuracy of the line parameters depends mainly on the quality of the basis functions. So the basis functions should be carefully chosen to assure the reliability of the results.

A. The Global Basis Functions

The adopted basis functions for the ith conductor are

$$\rho_{ijm}(u_i) = (1 \pm u_i)^{\tau_q} + a_m(1 \pm u_i)^{\tau_{q+1}} + b_m(1 \pm u_i)^{\tau_{q+2}} \quad (9)$$

where $-1 \le u_i \le 1$. For odd (even) m, the plus (minus) sign is referred and $q = (m+1)/2$ ($q = m/2$). For horizontal surfaces $u_i = 2(x - x_{ic})/W_i$ with $x_{ic} = (x_{i3} + x_{i4})/2$ and for vertical ones $u_i = 2(y - y_c)/t$ with $y_c = t/2$. The constants a_m and b_m are specified according to $\rho_{ijm}(1) = \rho'_{ijm}(1) = 0$ for odd m and $\rho_{ijm}(-1) = \rho'_{ijm}(-1) = 0$ for even m. τ_q is the power of the first term of the mth basis function used to characterize the asymptotic behavior of the charge distribution near the conducting corner. For the corners at $y = t$, $\tau_q = 2q/3 - 1$ [15]. Note that $\tau_1 \equiv \tau_{10} = -1/3$ which guarantees that the charge distribution has singularity as $\delta^{-1/3}$ as u_i approaches -1 and $+1$ for odd and even m, respectively. Note that the asymptotic behavior of the charge distribution near the edges at $y = 0$, when $\epsilon_r > 1$, is different from that at $y = t$. From [16], one can obtain

$$\tau_1 \equiv \tau_{1r} = 2/\pi \tan^{-1}\sqrt{1 + 2/\epsilon_r} - 1 \quad (10)$$

for the conductor corners at $y = 0$. The results obtained by these two τ_1 values will be compared in the next section.

The derivation of the bases (9) is similar to that reported in [15]. Extensive studies have been done [15] for the bases incorporated in the full-wave SDA in analyzing coupled thin microstrip lines. It has been found that the bases are capable of providing smooth current distributions and accurate field solutions even if the lines are electrically wide and strongly coupled. The performance of the basis functions (9) as applied to thick microstrip problems will be investigated later.

B. Numerical Details of the Single and Double Integrals

The matrix $\underline{M}$ in the final matrix equation (6) is symmetric. Thus, only the entries in the upper triangle need computing. If $K_b = 2N_b$ bases are used for each surface in a single-conductor problem, $(4N_b)^2$ single integrals and $(4N_b)(4N_b + 1)/2$ double integrals are involved for each spectral variable α_n. It may take a long time to calculate these entries. To minimize the computing time, an efficient way must be used.

1) Single Integrals: The y-dependence of the Green's function $G_{jk}(y)$ in the one-dimensional integrals in (5) can be a linear combination of either $\cosh\alpha_n y$ and $\sinh\alpha_n y$ or $\cosh\alpha_n(t - y)$ and $\sinh\alpha_n(t - y)$, $0 \le y \le t$. Substituting one of the three terms of the bases in (9) into (5) and using exponential functions to replace the hyperbolic functions, one can find that all the single integrals fall into the following two categories:

$$I_1(\Omega, \tau) = \int_0^1 e^{-\Omega u} u^\tau\,du \quad (11a)$$

$$I_2(\Omega, \tau) = \int_0^1 e^{-\Omega u}(1-u)^{\tau}\, du \tag{11b}$$

where $\Omega = |\alpha_n|t$. The closed form expressions for I_1 and I_2 can be easily derived for small and large arguments. Note that for the mth basis function in (9) the single integral becomes

$$I_{sm}(\Omega) = I_s(\Omega, \tau_q) + a_m I_s(\Omega, \tau_{q+1}) + b_m I_s(\Omega, \tau_{q+2}) \qquad s = 1, 2. \tag{12}$$

2) Double integrals: In a fashion similar to the derivation of (11), each double integral in (5) is found to be weighted sums of the following three types of integrals

$$D_{1jk}(\Omega) = \int_0^1 \int_0^1 e^{-\Omega|u-v|} \begin{Bmatrix} (1-u)^{\tau_j} \\ u^{\tau_j} \end{Bmatrix} \begin{Bmatrix} (1-v)^{\tau_k} \\ v^{\tau_k} \end{Bmatrix} du\, dv \tag{13a}$$

$$D_{2jk}(\Omega) = e^{-\Omega} \cdot \int_0^1 \int_0^1 e^{-\Omega(1-|u-v|)} \begin{Bmatrix} (1-u)^{\tau_l} \\ u^{\tau_j} \end{Bmatrix} \begin{Bmatrix} (1-v)^{\tau_k} \\ v\tau_k \end{Bmatrix} du\, dv \tag{13b}$$

$$D_{3jk}(\Omega) = \begin{Bmatrix} I_1(\Omega, \tau_j) \\ I_2(\Omega, \tau_j) \end{Bmatrix} \begin{Bmatrix} I_1(\Omega, \tau_k) \\ I_2(\Omega, \tau_k) \end{Bmatrix}. \tag{13c}$$

The absolute value operations in the exponents reflect the fact that the Green's functions $G_{jk}(y, \xi)$ have different expressions for $y > \xi$ and $y < \xi$. The value of Ω can range from zero to a large one, depending on how thick the strip is and where the spectral summation is truncated, so the simple closed forms for D_{1jk} and D_{2jk} with sufficient accuracy are nearly impossible to obtain. On the other hand, if (13a) and (13b) are expanded into double infinite series, the results converge quickly for $\Omega < 1$. But it will take a long time to calculate the data for $\Omega > 1$. An efficient way to evaluate these integrals when the program is being executed is to use a database in readiness as described below.

3) The database and the interpolation: Two one-dimensional integration routines, which are capable of handling singularities at both upper and lower integration limits, are employed to calculate the integrals sampled at $\Omega = 0, 0.125, 0.25, \cdots, 250$. D_{2jk}'s are calculated up to $\Omega = 50$ and neglected for $\Omega > 50$. The memory required to store these samples, for $N_b = 4$ and 10-digit accuracy and for both the single and double integrals, is about 3.5 megabytes. The Lagrange eight-point interpolation formula [17] is used to approximate the integrals based on these samples. It can be expected that only a small portion of CPU time is used for the computation of this part (the entries in $\underline{M}$ involving one- and two-dimensional integrations) when the program is being executed.

The values of D_{1jk} need evaluating for $\Omega > 250$ for some special cases. The integrals are first analytically changed to

$$D_{1jk}(\Omega) = \frac{1}{2^{\tau_j+\tau_k+1}} \int_0^1 e^{-\Omega u} g_{jk}(u)\, du \tag{14a}$$

where

$$g_{jk}(u) = \int_u^{2-u} \begin{Bmatrix} (2-v-u)^{\tau_j} \\ (v+u)^{\tau_j} \end{Bmatrix} \begin{Bmatrix} (2-v+u)^{\tau_k} \\ (v-u)^{\tau_k} \end{Bmatrix} dv. \tag{14b}$$

Then a set of 257-point equidistant samples of $g_{jk}(u)$ are calculated within $0 \le u \le 0.1$, and the integrals are approximated by the Simpson's rule [17]. Note that the values of g_{jk} are significant only when u is small. That is the very reason why 0.1 instead of 1 is used as the upper limit of the samples.

IV. Results

In this section, a convergence study is performed for the line parameters for a pair of closely coupled thick strips to indicate the numbers of basis functions and spectral terms required in the SDA program to obtain reliable data from the computer simulation. Then, to validate the proposed technique, the calculated microstrip characteristic impedances are compared with those obtained by other theoretical technique and available measured data. The soundness of the proposed technique is further demonstrated by investigating the trend of the capacitance values for a particular coupled-line obtained by the multistrip model, with model parameters being successively pushed to near the numerical extremities. Finally, the influence of finite metallization thickness on the line parameters of a four-line coupled microstrip structure is presented and discussed.

A. Convergence Study and Numerical Efficiency

A pair of coupled microstrips with aspect ratios $w : t : s = 0.2 : 1 : 0.1$ is used to examine the performance of the employed global bases in (9) incorporated into the SDA. The ratios are chosen to provide a rigorous test for the SDA program to achieve accurately converged results for both odd- and even-mode excitations.

Fig. 2(a) and (b) plots, respectively, the effective dielectric constants and characteristic impedances for the coupled lines against the normalized number of spectral summation terms, $N' = Nh_1/A$, included in the calculation for different values of N_b. The size of the matrix $\underline{M}$ in (6) is $8N_b \times 8N_b$. For reference, the dashed lines in the figure show the boundaries for $\pm 0.05\%$ deviations from the nearly converged data using $N_b = 4$ and $N' = 5 \times 10^3$.

The solid lines are the results using $\tau_1 = \tau_{1r}$ given in (12) and the dotted lines using $\tau_1 = \tau_{10}$ for the first basis function in (9). Note that the values of a_1 and b_1 in (9) are different for both τ_1 values and that τ_{10} is used for the edges at $y = 0$ when C_0 is calculated. All the higher order terms use the same powers, i.e., $\tau_q = 2q/3 - 1$ for $q > 1$. As indicated in Fig. 2(a) and (b), 1) for $N_b = 3$ and 4, the nearly converged results for both τ_1 values have less than 0.01% discrepancies, and 2) $N_b = 3$ and $N' \approx 2 \times 10^3$ are needed to obtain solutions within the $\pm 0.05\%$ boundaries. Also of interest, but not shown here, is that similar convergence conditions have been obtained for the case with $t = 0.1$, $s = 0.025$, with all the other parameters remaining unchanged. Since the numerical reliability has been

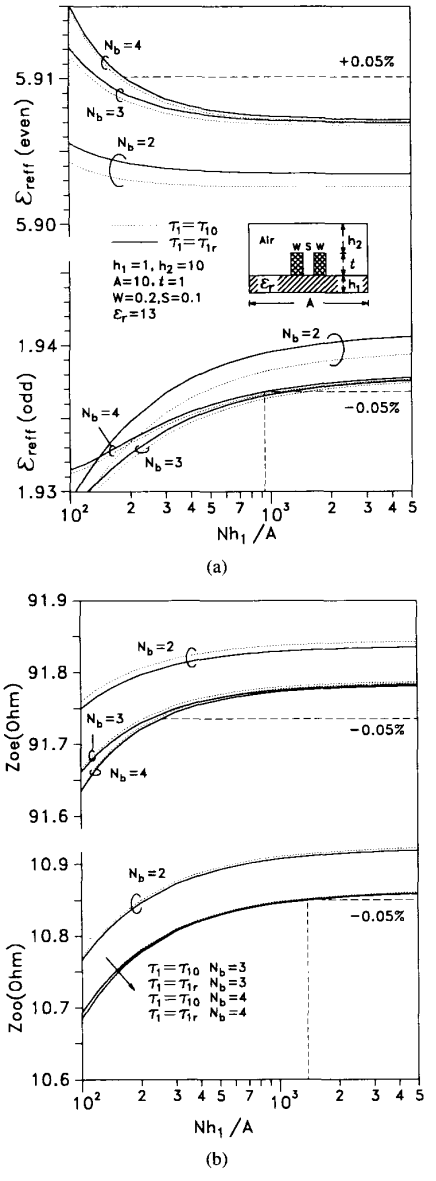

Fig. 2. Convergence study for the line parameters of a pair of closely coupled thick microstrip lines for even- and odd-mode excitations. (a) Effective dielectric constants. (b) Characteristic impedance.

established, 1) $\tau_1 = \tau_{10}$, for each substrate dielectric constant used here, 2) $N_b = 3$ and 3) $N' = 2 \times 10^3$ are used for calculation of results. Note that i) can reduce the preprocessing tasks and memory for the integration database.

The program is executed on an IBM 320 workstation. No asymptotic expression for the Green's function, such as that in [12], or transformed basis function is used. For zero-thickness microstrip, it takes eight seconds to calculate the line parameters for $N_b = 3$ and 2×10^4 ($N' = 2 \times 10^3$ using $A/h_1 = 10$) spectral summation terms. For the present technique, where the order of the final matrix is increased by a factor of 4, it takes 64 seconds to calculate the results and 30 seconds to read the integration database.

TABLE I
COMPARISON OF CHARACTERISTIC IMPEDANCE VALUES OF THICK MICROSTRIPS. STRUCTURAL PARAMETERS: $\epsilon_r = 4.7$, $t = 2.8$

h_1	w	Measurement [18]	Theory in [7]	This work
8	10	53	–	56.03
8	15	42.5	–	45.64
8	20	36	–	38.64
14	10	73	–	73.35
14	15	61	61.8	62.03
31	5	116	118.4	118.6
31	10	102	–	99.93
31	15	90.5	87.8	88.12
31	20	81	79.2	79.48
60	3.7	151	–	148.8
60	10	125.4	–	122.7
60	15	111	–	110.8

B. Comparison with Other Theory and Available Measured Data

It is necessary to examine if the converged results computed by the SDA program are correct. The structure shown in Fig. 1 can be used to simulate an open microstrip line using relatively large values of S, h_2 and A as compared with strip width and substrate height. Table I compares the calculated characteristic impedances with those provided by the Green's function method [7] and experimental measurement [18]. The strip thickness $t = 2.8$ and substrate relative dielectric constant $\epsilon_r = 4.7$. Among the case studies listed in the table, the strip width to substrate thickness ratio covers from 0.06–2.5 and strip thickness to the strip width ratio from 0.14–0.76. As shown in the table, both theoretical techniques have closer values, and the calculated and measured results show reasonable agreement.

C. Comparison with the Multistrip Model

The two-level model [10] and the multistrip model [11] are important milestones for the approximate analyses of finite thickness microstrip lines. Using these models, the formulation can be significantly simplified and the results can be efficiently obtained. For example, if the SDA is used, neither double nor single integral is involved in the final matrix. In the multistrip model, the boundary condition on the strip sidewalls is simulated by pairs of narrow strips at different levels. If the width of these narrow strips could be reduced to zero and the number of levels could be increased to infinity, the simulated boundary condition would be as ideal as that is formulated in Section II. Thus, in this subsection, the model is investigated extensively to show how narrow the width is and how many the number of the levels is sufficient to obtain the accurately converged results. The coupled lines in [11] is used as the test configuration and the result calculated by the proposed technique is referred as the accurately converged solution.

Fig. 3 compares the referred odd-mode capacitance value with those presented in [11, Fig. 5], where the converged results are given only up to eight levels. Note that the referred result is irrelevant to the number of metallization levels. The results from both approaches deviate from each other by about 10%, which is a large value for many applications. Thus,

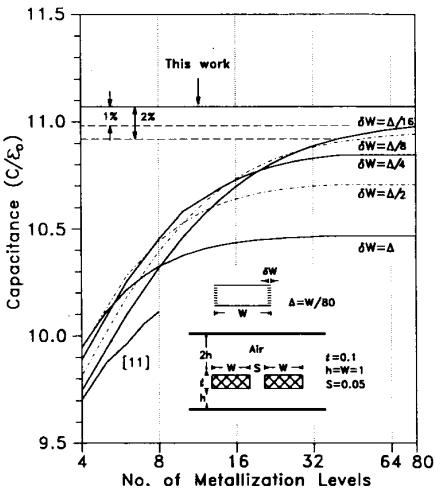

Fig. 3. Comparison of calculated odd-mode capacitance for suspended coupled lines with those obtained by the multistrip model.

it is necessary to investigate what happens in between. The investigation is done by successively reducing the width of the inner level strips and increasing the number of levels to check if the results can approach to the referred value.

The test widths of the inner level strips are $\delta W = \Delta$, $\Delta/2$, $\Delta/4$, $\Delta/8$, and $\Delta/16$, where $\Delta = W/80$. The results for each width are calculated up to 80 levels. The standard SDA for infinitely thin conductors is employed to assist the investigation. The basis functions in [15] are used as the basis and test functions for the charge densities on the top and bottom levels and rectangular pulses for the inner strips. To obtain converged field solutions, $N' = 10^4$ is required for $\delta W = \Delta$, $\Delta/2$, and $\Delta/4$ and $N' = 2 \times 10^4$ for $\delta W = \Delta/8$ and $\Delta/16$. Note that the matrix size for the multistrip model is close to double the number of strip levels.

The plots for $\delta W = \Delta$ and $\Delta/2$ reach the converged values at 16 and 24 levels, respectively. As the inner strips get narrower up to $\Delta/8$, more levels are required for convergence, and the nearly converged values increase. It should be noted that insufficiently small value of δW leads to a result with poor accuracy even when a large number of levels is used.

The results for $\delta W = \Delta/8$ and $\Delta/16$ at 40 levels have 2% deviation from the referred data. The deviation is further investigated as follows. First, the rectangular pulse may not be a good choice to model the charge density on the inner strip, since the charge densities on the inner strips away from the lateral walls should be vanished. Right-angled triangular basis functions are thus used. Only 10% of the deviation is reduced, i.e., the capacitance value has 1.8% deviation from the referred result. Second, the number of levels is increased from 40 to 80. As shown in Fig. 3, the deviation is reduced to 1%. It indicates, again, that the role the number of levels plays in the convergence process is important. Note that each inner strip, if sufficiently narrow, can be looked as a matching "point" that satisfies the boundary condition on the conductor surfaces in the vertical direction. So, that more and more "points" are required to support the convergence means that the matching quality of the boundary condition is closer and closer to the ideal case. Thus, by method of induction, it can be concluded that the results obtained by the multistrip model, with both sufficiently small δW and a sufficient number of metallized levels, do approach to that obtained by the proposed technique.

D. The Influence of Finite Metallization Thickness on the Propagation Characteristics of Multiple Coupled Microstrip Lines

In this subsection, the proposed technique is employed to investigate the influence of finite metallization on the line characteristics of multiple coupled microstrip lines. Fig. 4 shows the results for a four-line microstrip structure, in which the lines are of equal widths and equidistantly spaced. The structure has four eigenmodes with effective dielectric constants ϵ_{reffi}, $1 \leq i \leq 4$, eigenvoltage vectors of relative amplitudes $(1e_1e_11)$, $(1e_2 - e_2 - 1)$, $(1 - e_3 - e_31)$, and $(1 - e_4e_4 - 1)$, which are referred to as modes 1, 2, 3, and 4, respectively. The modes are identified as their ϵ_{reff} values in a descending order as shown in Fig. 4(a). All the effective dielectric constants decrease as the thickness is increased. Mode 1 has the least variation of ϵ_{reff} value due to the change of metallization thickness, whereas mode 4 has the most vairation. The ϵ_{reff} values of modes 2, 3, and 4 are more and more influenced by the change of t when the strips get closer and closer. Note that the plots for ϵ_{reff2}, ϵ_{reff3}, and ϵ_{reff4} change quickly when S is further decreased from 0.1.

The variations of mode amplitudes in response to the change of t values are plotted in Fig. 4(b). The values of e_i are important for analyzing crosstalk produced on the lines in the multiconductor transmission-line system. Due to the increase of the strip thickness, the value of e_4 varies significantly, but those of e_1, e_2, and e_3 vary just perceptibly.

The entries in characteristic conductance matrix $\underline{G}$ for different values of t are plotted in Fig. 4(c). Due to the reciprocity relation and the symmetry of the structure, only G_{1j}, $1 \leq j \leq 4$, G_{22} and G_{23} need to be specified. G_{13} and G_{14} are not plotted here, since their magnitudes are much smaller than the others'. Note that the values of G_{ij} are positive for $i = j$ and negative for $i \neq j$. The magnitude of each entry increases as the thickness is increased. Significant increases of the G_{ij} values are found when the line spacing is small. When the spacing is larger than two times the strip width, each conductance plot approaches its flat part. The results shown in Fig. 4 indicate that the influence of finite metallization on the circuit parameters of multiple microstrip lines is important, especially when the lines are closely coupled.

V. Conclusion

The spectral domain approach (SDA) has been successfully applied to analyze single and coupled microstrip lines with arbitrary metallization thickness. The infinitesimal thickness for the strip conductor is no longer a limitation on the applicability of the SDA technique.

In the analysis, the legitimacy of the extended SDA incorporated with the applied basis functions is validated through the demonstration of its capability of providing accurately con-

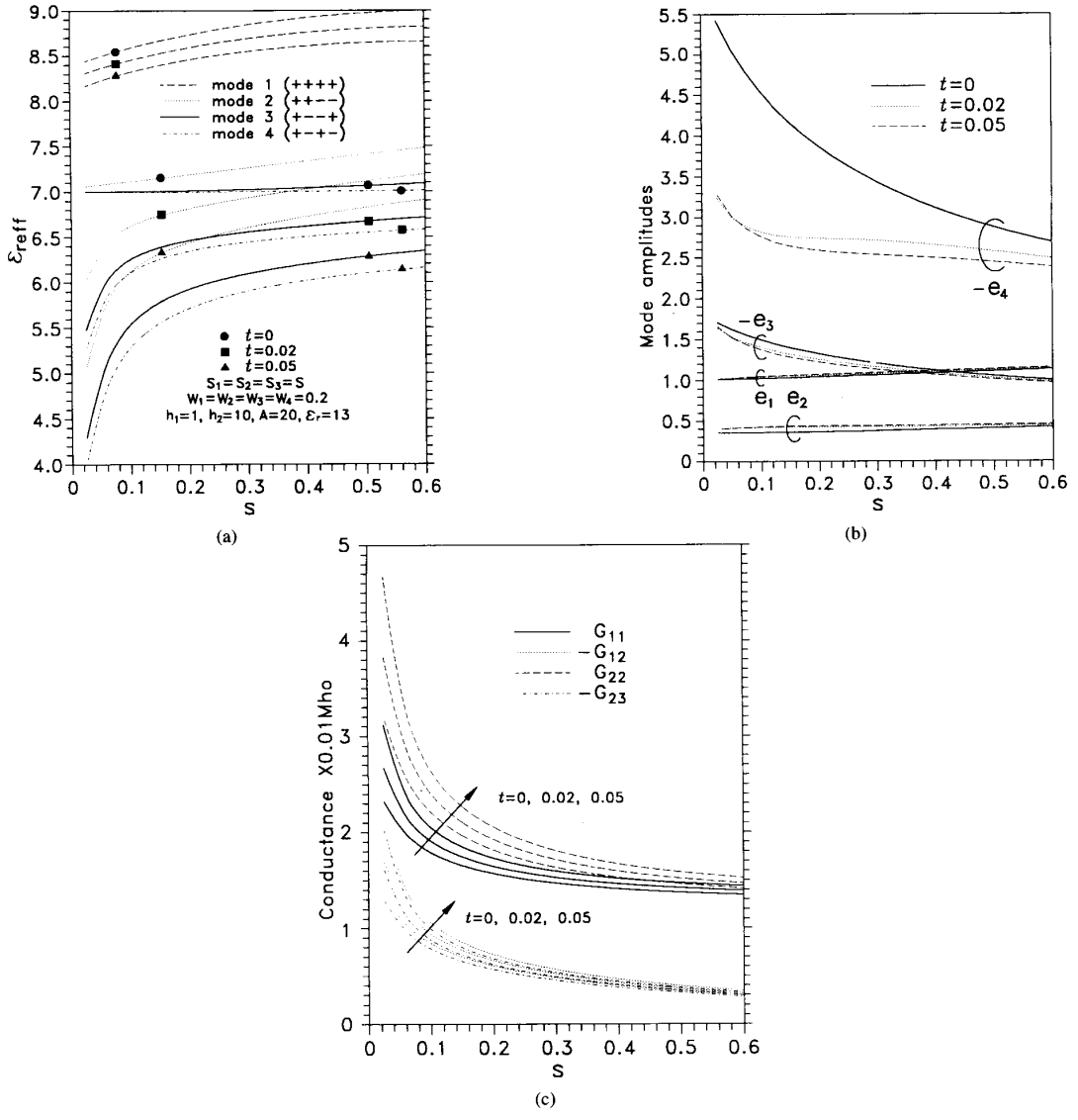

Fig. 4. Influence of finite metallization thickness on the line parameters of a four-line coupled microstrip structure. (a) Effective dielectric constants. (b) Relative magnitudes of eigenvoltage vectors. (c) Entries of the characteristic conductance matrix.

verged results for closely coupled thick microstrip lines using a small matrix. The extensive investigation into the multistrip model shows that the results with structural parameters being pushed to the extremities do approach to the converged result obtained by the proposed technique. For multiple coupled microstrip lines, line parameters for different eigenmodes are influenced by the finnite metallization thickness in different ways. The importance of the responses of the line characteristics to the change of finite metallization thickness should be specially emphasized when the lines are closely packed.

ACKNOWLEDGMENT

The author would like to thank Prof. C.-K. C. Tzuang for valuable suggestions at the beginning of the project execution, and to thank the reviewers for their constructive comments.

REFERENCES

[1] T. Itoh, Ed., *Planar Transmission Line Structures.* New York: IEEE Press, 1987.
[2] T. C. Edwards, *Foundations for Microstrip Circuit Design.* 2nd ed. New York: Wiley, 1992.
[3] P. Daly, "Hybrid-mode analysis of microstrip by finite-element methods," *IEEE Trans. Microwave Theory Tech.*, vol. MTT-19, pp. 19–25, Jan. 1971.
[4] C. Shih *et al.*, "Frequency-dependent characteristics of open microstrip lines with finite strip thickness," *IEEE Trans. Microwave Theory Tech.*, vol. 37, pp. 793–795, Apr. 1989.
[5] L. Zhu and E. Yamashita, "Full-wave boundary integral equation method for suspended planar transmission lines with pedestals and finite metallization thickness," *IEEE Trans. Microwave Theory Tech.*, vol. 41, pp. 478–483, Mar. 1993.
[6] H. A. Wheeler, "Transmission-line properties of parallel strips separated by a dielectric sheet," *IEEE Trans. Microwave Theory Tech.*, vol. MTT-13, pp. 172–185, Mar. 1965.

[7] E. Yamashita and K. Atsuki, "Analysis of thick-strip transmission lines," *IEEE Trans. Microwave Theory Tech.*, vol. MTT-19, pp. 120–122, Jan. 1971.
[8] T.-N. Chang and C-H. Tan, "Analysis of a shielded microstrip line with finite metallization thickness by the boundary element method," *IEEE Trans. Microwave Theory Tech.*, vol. 38, pp. 1130–1132, Aug. 1990.
[9] E. Yamashita, "Variational method for the analysis of microstrip-like transmission lines," *IEEE Trans. Microwave Thory Tech.*, vol. MTT-16, pp. 529–535, Aug. 1968.
[10] R. T. Kollipara and V. K. Tripathi, "Quasi-TEM spectral domain technique for multiconductor structures with rectangular and trapezoidal conductor cross sections," *Microwave Optical Technology Lett.*, vol. 3, pp. 4–6, 1990.
[11] E. Drake, F. Medina, and M. Horno, "Quasi-TEM analysis of thick multistrip lines using an efficient iterative method," *Microwave Optical Technology Lett.*, vol. 5, no. 10, pp. 530–534, Sept. 1992.
[12] F. Olyslager, N. Faché, and D. De Zutter, "New fast and accurate line parameter calculation of general multiconductor transmission lines in multilayered media," *IEEE Trans. Microwave Theory Tech.*, vol. 39, no. 6, pp. 901–909, June 1991.
[13] G. G. Gentili and G. Macchiarella, "Quasi-static analysis of shielded planar transmission lines with finite metallization thickness by a mixed spectral-space domain method," *IEEE Trans. Microwave Theory Tech.*, vol. 42, pp. 249–255, Feb. 1994.
[14] T. Itoh, Ed., *Numerical Techniques for Microwave and Millimeter-wave Passive Structures.* New York: Wiley, 1989.
[15] J.-T. Kuo and C.-K. C. Tzuang, "Complex modes in shielded suspended coupled microstrip lines," *IEEE Trans. Microwave Theory Tech.*, vol. 38, pp. 1278–1286, Sept. 1990.
[16] R. Mittra and S. W. Lee, *Analytical Techniques in the Theory of Guided Waves.* New York: Macmillan, 1971.
[17] M. Abramowitz and I. A. Stegun, Eds., *Handbook of Mathematical Functions with Formulas, Graphs, and Mathematical Tables.* New York: Dover, 1964.
[18] H. R. Kaupp, "Characteristics of microstrip transmission lines," *IEEE Trans. Electron. Comput.*, vol. EC-16, pp. 185–193, Apr. 1967.

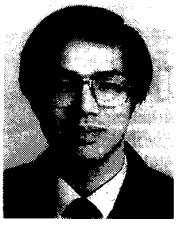

Jen-Tsai Kuo (S'89–M'93) received the B.S. degree in communication engineering from the National Chiao Tung University (NCTU) in 1981 and the M.S. degree in electrical engineering from the National Taiwan University in 1984, both in Taiwan, R.O.C. In 1992, he received the Ph.D. degree from the NCTU.

Since 1984, he has been with the Department of Communciation Engineering at the NCTU as a Lecturer at the Microwave and Communication Electronics Laboratory. His current research interests include the analysis and design of microwave and millimeter-wave circuits and high-speed interconnects and packages, field-theoretical study of guided waves, and numerical techniques in electromagnetics.